FRATS: Functional Regression Analysis of DTI Tract Statistics

Hongtu Zhu*, Martin Styner, Niansheng Tang, Zhexing Liu, Weili Lin, and John H. Gilmore

Abstract—Diffusion tensor imaging (DTI) provides important information on the structure of white matter fiber bundles as well as detailed tissue properties along these fiber bundles *in vivo*. This paper presents a functional regression framework, called FRATS, for the analysis of multiple diffusion properties along fiber bundle as functions in an infinite dimensional space and their association with a set of covariates of interest, such as age, diagnostic status and gender, in real applications. The functional regression framework consists of four integrated components: the local polynomial kernel method for smoothing multiple diffusion properties along individual fiber bundles, a functional linear model for characterizing the association between fiber bundle diffusion properties and a set of covariates, a global test statistic for testing hypotheses of interest, and a resampling method for approximating the *p*-value of the global test statistic. The proposed methodology is applied to characterizing the development of five diffusion properties including fractional anisotropy, mean diffusivity, and the three eigenvalues of diffusion tensor along the splenium of the corpus callosum tract and the right internal capsule tract in a clinical study of neurodevelopment. Significant age and gestational age effects on the five diffusion properties were found in both tracts. The resulting analysis pipeline can be used for understanding normal brain development, the neural bases of neuropsychiatric disorders, and the joint effects of environmental and genetic factors on white matter fiber bundles.

Index Terms—Diffusion tensor imaging, fiber bundle, functional regression, global test statistic, registration.

I. INTRODUCTION

WATER molecules in the human brain diffuse preferentially along the major axis of white matter fiber bundles. Thus, diffusion tensor imaging (DTI), which can track the effective diffusion of water in the human brain *in vivo*, is used to accurately map *in vivo* the structure and orientation of fiber tracts in the white matter of the brain [1], [2]. The directional dependence of water diffusion in each voxel can be characterized by a matrix, called a diffusion tensor (DT), and the degree of diffusivity can be quantified by using the three eigenvalue-eigenvector pairs of DT and its related parameters, such as fractional anistropy (FA) [3]–[6]. There has been a wealth of neuroimaging studies using a set of water diffusion related parameters including FA, mean diffusivity (MD), and the three eigenvalues of diffusion tensor as a marker for white matter tract maturation and integrity found in [7]–[10], and many others. Analyzing these water diffusion related parameters across subjects requires specific statistical methods for the group analysis of diffusion imaging data.

In the current literature, three major approaches to the group analysis of diffusion imaging data are region-of-interest (ROI) analysis, voxel based analysis, and fiber tract based analysis [11]–[13]. The region-of-interest (ROI) method used in some neuroimaging studies [14], [15] primarily averages diffusion properties in some manually drawn ROIs for each subject and then creates a single statistic per ROI [13]. Some major drawbacks of ROI analysis are the difficulty in identifying meaningful ROIs, particularly the long curved structures common in fiber tracts, the instability of statistical results obtained from ROI analysis, and the partial volume effect in relative large ROIs. The ROI method is also based on a stringent assumption that diffusion properties in all voxels of the same ROI are essentially homogeneous, which is largely false for DTI.

Voxel based analysis is used more commonly than ROI analysis in neuroimaging studies [16]–[19]. The first step involves fitting a statistical model to the smoothed and registered diffusion properties imaging data from multiple subjects at each voxel to generate a parametric map of test statistics (or *p*-values). The second step is to correct for the multiple comparisons across the many voxels of the imaging volume [20]–[22]. It suffers from issues of alignment quality and the arbitrary choice of smoothing extent [11], [20], [23], [24]. As shown in [24], the final results of voxel-based analysis can strongly depend on the amount of smoothing in the smoothed diffusion imaging data.

With the drawbacks mentioned of ROI and voxel based analysis, there is a growing interest in the DTI literature in developing fiber tract based analysis of diffusion properties, such as eigenvalues and fractional anisotropy (FA) values [11], [12], [25], [26]. For instance, Smith *et al.* develop a *tract-based spatial statistics* framework for constructing local diffusion properties along the white matter skeleton followed by performing pointwise hypothesis tests on the skeleton [11]. Yushkevich and coauthors propose a model-based framework for the statistical

*H. Zhu is with the Department of Biostatistics, and Biomedical Research Imaging Center, University of North Carolina at Chapel Hill, Chapel Hill, NC 27599 USA (e-mail: hzhu@bios.unc.edu).

M. Styner, Z. Liu, and J. H. Gilmore are with Department of Psychiatry, University of North Carolina at Chapel Hill, Chapel Hill, NC 27599 USA.

N. Tang is with Department of Statistics, Yunnan University, Kunming, 650091 Yunnan, China.

W. Lin is with Department of Radiology, University of North Carolina at Chapel Hill, Chapel Hill, NC 27599 USA.

analysis of diffusion properties on the medial manifolds of fiber tracts followed by testing pointwise hypotheses on the medial manifolds [25]. Similar to the work proposed in this paper, Goodlett *et al.* propose to use a functional data analysis method to compare a univariate diffusion property, such as fractional anisotropy, across two (or more) populations for a single hypothesis test per tract [26]. Their method is limited to a univariate diffusion property and cannot control for other covariates of interest, such as age, gender, and behavioral variables. Moreover, the permutation test and the Hotelling T^2 statistic used in [26] may be statistically oversensitive, because only the data in the reduced principal component analysis space are permuted. Statistically, such a procedure, which ignores substantial noise in the original data, can lead to misleading results.

What these three methods do not account for is the comparison of fiber bundle diffusion properties across groups and the development of fiber bundle diffusion properties along time, while controlling for other covariates of interest, such as gender [11], [14], [16]–[19]. Making these comparisons requires a regression modeling framework for the analysis of fiber bundle diffusion properties and a set of covariates of interest, such as age, diagnostic status, and gender. This paper presents a functional regression analysis of DTI tract statistics, called FRATS, for modeling the relationship between fiber bundle diffusion properties and covariates of interest. Compared with [26] and other existing literature, there are four methodological contributions in this paper. First, the local polynomial kernel method is used to regularize multiple diffusion properties along individual fiber bundles. Second, a functional linear model is developed to characterize the association between fiber bundle diffusion properties and any covariate of interest. Third, a global test statistic is proposed for testing hypothesis of interest. Fourth, a resampling method is developed for estimating the p-value of the global test statistic. The proposed methodology is used to characterize the development of five diffusion properties along the splenium and right internal capsule tracts in a clinical study of neurodevelopment in the University of North Carolina at Chapel Hill.

II. METHODS

This paper introduces a set of statistical tools for the group analysis of fiber bundle diffusion properties while controlling for a set of covariates of interest. Comparing diffusion properties in populations of DTIs requires imaging methods for establishing correspondence among regions of anatomy in DTIs. For this purpose, we use the DTI atlas building methods proposed in [26], which are included here for completion. The focus of this paper is to develop the functional regression model pipeline, called FRATS, for assessing the association between fiber bundle diffusion properties and covariates of interest.

A. DTI Atlas Building

Before applying FRATS, a quality control pipeline is applied to each of the subjects' diffusion weighted images (DWIs) to check if the DWIs contain large slice brightness artifacts, intra-gradient Venetian blind artifacts, and motion artifacts

using DTIPrep.[1] Skull stripping is then performed automatically via a brain mask computed from both the nondiffusion weighted baseline image and isotropic diffusion weighted image using a free software itkEMS.[2] Masking out the nonbrain tissues stabilizes the subsequent DTI estimation and registration step. Diffusion tensors are estimated for each subject from a series of cleaned diffusion weighted images using a weighted least square tensor estimation [2], [27].

After DTI estimation, registration occurs and its accuracy is crucial for identifying meaningful group differences. We use a nonlinear fluid deformation based high-dimensional, unbiased atlas computation method to carry out a large deformation nonlinear registration [28]. The atlas building procedure is initialized by an affine registration and followed by a nonlinear registration of a feature image which is sensitive to the geometry of white matter. Further reference of the DTI atlas building procedure has been described in [26]. Then, we warp each of the tensor images into the unbiased space and reorient them using the finite strain approximation proposed by [29] to get the aligned DTIs. After averaging all the registered DTIs, a study specific unbiased DTI atlas is created. The tensor warping and averaging are performed using a novel Log-Euclidean geometry [30].

Major fiber bundles are tracked in the atlas space within 3D Slicer.[3] First, ROIs are drawn with the Editor module and then fibers are tracked using a stream line method with the Tractography module. Usually, the fibers directly generated in this way contain some fibers not belonging to the bundle that we are interested in due to either the noise in DTI data or not proper ROI delineation. We use FiberViewer to visualize and clean the fibers. Tractography of atlas fiber bundles are more reliable than individual ones because of the improved signal-to-noise ratio of the atlas.

With the fiber bundles in atlas space, each subject's DTI data is transformed into the atlas space. When transforming the diffusion properties from native space to the atlas space, tri-linear interpolation is used to interpolate diffusion properties from the native space. Finally, we get a set of individual tracts with corresponding geometry but varying diffusion properties. Within FiberViewer, a cutting plane is first placed perpendicular to the fibers at a location where the fibers are organized neatly to define the origin of arc length. The diffusion properties along fiber tracts are then measured and plotted as functions of arc length. Using FiberViewer, these plots from each subject are generated. This allows us to conduct a group comparison analysis of the along-bundle tensor properties. Except for 3D Slicer, all DTI tools and itkEMS are part of the open source UNC NeuroLib software repository.[1]

B. FRATS: Nonparametric Model

After spatial normalization of tensor images, we propose to use a functional regression model to analyze diffusion properties along the same fiber bundle from multiple subjects. FRATS consists of four major components: a regularization of individual

---

[1]http://www.ia.unc.edu/dev

[2]http://www.ia.unc.edu/dev/download/itkems
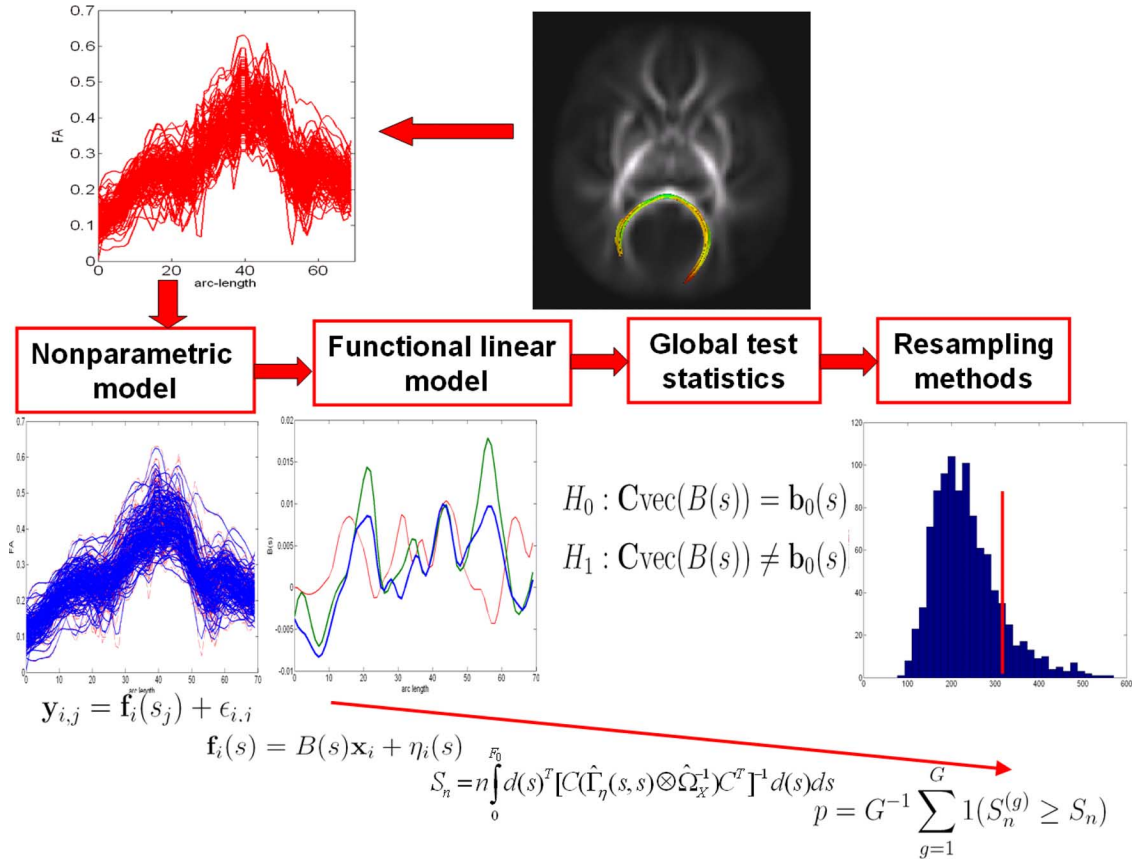
[3]http://www.slicer.org

Fig. 1. A schematic overview of FRATS: a nonparametric model for regularizing individual tracts, a functional linear model, a global test statistic for hypothesis testing, and a resampling method for estimating the p-value of the global test statistic.

tracts, a functional linear model, a global test statistic for hypothesis testing, and a resampling method for estimating the p-value of the global test statistic. A schematic overview of FRATS is in Fig. 1. We describe each of these components in detail below.

To regularize individual tracts, we develop a *nonparametric model* for multiple diffusion properties (e.g., FA) along the same fiber bundle as a smooth function of arc length from each subject as follows. For the ith subject, we consider a $m \times 1$ vector of diffusion properties, denoted by $\mathbf{y}_{i,j} = (y_{ij,1}, \ldots, y_{ij,m})^T$, and its associated arc length s_j for the jth location grid point on the fiber bundle for $j = 1, \ldots, L_0$ and $i = 1, \ldots, n$, where L_0 and n denote the numbers of grid points and subjects, respectively. The nonparametric model is given by

$$\mathbf{y}_{i,j} = \mathbf{f}_i(s_j) + \epsilon_{i,j}, \tag{1}$$

where $\mathbf{f}_i(s) = (f_{i,1}(s), \ldots, f_{i,m}(s))^T$ is an $m \times 1$ vector of continuous functions with second-order continuous derivative, $E[\mathbf{y}_{i,j}|\mathbf{f}_i(s_j)] = \mathbf{f}_i(s_j)$, and $\text{Cov}[\mathbf{y}_{i,j}|\mathbf{f}_i(s_j)] = \Sigma(s_j)$. Our aim is to reconstruct the continuous function vector $\mathbf{f}_i(s)$ based on observed fiber bundle diffusion properties.

To simultaneously construct all individual function vectors $\mathbf{f}_i(s)$, we develop an adaptive *local polynomial kernel smoothing* technique [31]–[36]. Specifically, using Taylor's expansion, we can expand $\mathbf{f}_i(s_j)$ at s to obtain

$$\mathbf{f}_i(s_j) = \mathbf{f}_i(s) + \dot{\mathbf{f}}_i(s)(s_j - s) = \mathbf{A}_i \mathbf{z}_j, \tag{2}$$

where $\mathbf{z}_j = (1, s_j - s)^T$ and $\mathbf{A}_i = [\mathbf{f}_i(s) \ \dot{\mathbf{f}}_i(s)]$ is an $m \times 2$ matrix with $\dot{\mathbf{f}}_i(s) = d\mathbf{f}_i(s)/ds$. We develop an algorithm to estimate $\mathbf{A}_i$ as follows.

- Step (1.1) is to construct an initial estimate of $\mathbf{f}_i(s)$ for each i. Let $\mathbf{a}_{i;k}$ be the kth row of $\mathbf{A}_i$ and $K(\cdot)$ be a kernel function, such as the Gaussian, Epanechnikov, or uniform kernels [31]. Without loss of generality, we assume that the kernel function $K(\cdot)$ is always a symmetric probability density function. Throughout the paper, we take $K(t) = 0.75(1-t^2)\mathbf{1}(|t| \leq 1)$, where $\mathbf{1}(\cdot)$ is an indicator function. For each k and a fixed bandwidth h_k, we estimate $\mathbf{a}_{i;k}$ by minimizing an objective function given by

$$\sum_{j=1}^{L_0} (y_{ij,k} - \mathbf{a}_{i;k}^T \mathbf{z}_j)^2 K_{h_k}(s_j - s), \tag{3}$$

where $K_{h_k}(\cdot) = K(\cdot/h_k)/h_k$ is a rescaled kernel function. With some calculation, it can be shown that

$$\hat{\mathbf{a}}_{i;k} = \left[\sum_{j=1}^{L_0} \mathbf{z}_j K_{h_k}(s_j - s) \mathbf{z}_j^T \right]^{-1} \sum_{j=1}^{L_0} K_{h_k}(s_j - s) \mathbf{z}_j y_{ij,k}. \tag{4}$$

Let $\mathbf{e}_{1,2} = (1,0)^T$. Then, since $\mathbf{a}_{i;k} = (f_{i,k}(s), \dot{f}_{i,k}(s))^T$, $f_{i,k}(s)$ can be estimated by

$$\hat{f}_{i,k}(s) = \mathbf{e}_{1,2}^T \hat{\mathbf{a}}_{i;k} = \sum_{j=1}^{L_0} \tilde{K}_{h_k}^0(s_j - s, s) y_{ij,k} \tag{5}$$

where $\tilde{K}^0_{h_k}(\cdot, \cdot)$ are the empirical equivalent kernels [31]. Thus, $\hat{\mathbf{f}}_{i,k} = (\hat{f}_{i,k}(s_1), \ldots, \hat{f}_{i,k}(s_{L_0}))^T = S_{i,k}\mathbf{y}_{i:,k}$, where $\mathbf{y}_{i:,k} = (y_{i1,k}, \ldots, y_{iL_0,k})^T$ and $S_{i,k}$ is the smoother matrix for the kth measurement of the ith subject. For each k, we pool the data from all n subjects and select the optimal bandwidth h_k, denoted by $\hat{h}^{(1)}_{k,opt}$, by minimizing the generalized cross-validation score given by

$$\text{GCV}_k(h_k) = (n)^{-1} \sum_{i=1}^{n} \sum_{j=1}^{L_0} \frac{[y_{ij,k} - \hat{f}_{i,k}(s_j)]^2}{1 - L_0^{-1}\text{tr}(S_{i,k})}. \quad (6)$$

Based on the optimal $\hat{h}^{(1)}_{k,opt}$, we can estimate $\hat{f}_{i,k}(s)$ for all i.

- Step (1.2) is to construct an estimator of the covariance matrix $\Sigma(s_j)$ at s_j. Specifically, we consider the unbiased sample covariance matrix at s_j given by

$$\hat{\Sigma}(s_j) = (n - m)^{-1} \sum_{i=1}^{n} [\mathbf{y}_{i,j} - \hat{\mathbf{f}}_i(s_j)]^{\otimes 2} \quad (7)$$

where $\hat{\mathbf{f}}_i(s) = (\hat{f}_{i,1}(s), \ldots, \hat{f}_{i,m}(s))^T$ and $\mathbf{a}^{\otimes 2} = \mathbf{a}\mathbf{a}^T$ for any vector $\mathbf{a}$. It can be shown that $\hat{\Sigma}(s_j)$ converges to the true $\Sigma(s_j)$ in probability as both n and L_0 go to infinity.

- Step (1.3) is to compute an adaptive estimator of $\mathbf{f}_i(s)$ for all i using the initial results from Steps (1.1) and (1.2). For all k and a fixed bandwidth h, we estimate $\mathbf{A}_i$ by minimizing an objective function given by

$$\sum_{j=1}^{L_0} (\mathbf{y}_{ij} - \mathbf{A}_i\mathbf{z}_j)^T \hat{\Sigma}(s_j)^{-1} (\mathbf{y}_{ij} - \mathbf{A}_i\mathbf{z}_j) K_h(s_j - s). \quad (8)$$

Let $\mathbf{Z}_j = \text{block diagonal}(\mathbf{z}_j^T, \mathbf{z}_j^T, \ldots, \mathbf{z}_j^T)$ be an $m \times 2m$ matrix and $\mathbf{B}_i = (\mathbf{a}_{i;1}^T, \ldots, \mathbf{a}_{i;m}^T)^T$. It can be shown that

$$\hat{\mathbf{B}}_i = \left[\sum_{j=1}^{L_0} K_h(s_j - s) \mathbf{Z}_j^T \hat{\Sigma}(s_j)^{-1} \mathbf{Z}_j \right]^{-1}$$
$$\times \sum_{j=1}^{L_0} K_h(s_j - s) \mathbf{Z}_j^T \hat{\Sigma}(s_j)^{-1} \mathbf{y}_{ij}, \quad (9)$$

which leads to a new estimator of $f_{i,k}(s)$, denoted by $\hat{f}_{i,k}(s)^{\text{sec}}$ for each i and k. Let $\tilde{S}_{i,k}$ be the smoother matrix for the kth measurement of the ith subject such that $\hat{\mathbf{f}}_{i,k}^{\text{sec}} = (\hat{f}_{i,k}(s_1)^{\text{sec}}, \ldots, \hat{f}_{i,k}(s_{L_0})^{\text{sec}})^T = \tilde{S}_{i,k}\mathbf{y}_{i:,k}$. We pool the data from all n subjects and m measurements and select the optimal bandwidth h, denoted by $\hat{h}_{\text{opt}}$, by minimizing the generalized cross-validation score, denoted by $\text{GCV}(h)$, given by

$$\sum_{i=1}^{n} \sum_{j=1}^{L_0} \frac{[\mathbf{y}_{ij} - \hat{\mathbf{f}}_i(s_j)^{\text{sec}}]^T \hat{\Sigma}(s_j)^{-1} [\mathbf{y}_{ij} - \hat{\mathbf{f}}_i(s_j)^{\text{sec}}]}{n - n(mL_0)^{-1} \sum_{k=1}^{m} \text{tr}(\tilde{S}_{i,k})}, \quad (10)$$

where $\hat{\mathbf{f}}_i(s)^{\text{sec}} = (\hat{f}_{i,1}(s)^{\text{sec}}, \ldots, \hat{f}_{i,m}(s)^{\text{sec}})^T$. Based on the optimal $\hat{h}_{\text{opt}}$, we can estimate $\hat{f}_{i,k}(s)^{\text{sec}}$ for all i and k. Similar to the arguments in [35], it can be shown that when

$\Sigma(s)$ varies across s, $\hat{f}_{i,k}(s)^{\text{sec}}$ based on the optimal $\hat{h}_{\text{opt}}$ is more accurate than $\hat{f}_{i,k}(s)$ obtained from Step (1.1).

- Step (1.4) is to estimate the mean function $\mathbf{f}(s)$ and the covariance function $\Gamma(s, t)$ of $\mathbf{f}_i(s)$. Specifically, following [34], [36], we can estimate $\mathbf{f}(s)$ and $\Gamma(s, t)$ by using their empirical counterparts of the estimated $\hat{\mathbf{f}}_i(s)^{\text{sec}}$ as

$$\hat{\mathbf{f}}(s) = n^{-1} \sum_{i=1}^{n} \hat{\mathbf{f}}_i(s)^{\text{sec}} \quad (11)$$

and

$$\hat{\Gamma}(s, t) = n^{-1} \sum_{i=1}^{n} [\hat{\mathbf{f}}_i(s)^{\text{sec}} - \hat{\mathbf{f}}(s)][\hat{\mathbf{f}}_i(t)^{\text{sec}} - \hat{\mathbf{f}}(t)]^T. \quad (12)$$

The diagonal of $\Gamma(s, s)$ reflects the variance of $\mathbf{f}_i(s)$ at the location s.

C. FRATS: Functional Linear Model

We develop a *functional linear model* to characterize the relationship between all diffusion properties along fiber tracts and a set of covariates of interest, such as age, group, and gender. We assume that

$$\mathbf{f}_i(s) = B(s)\mathbf{x}_i + \eta_i(s), \quad i = 1, \ldots, n, \quad (13)$$

where $B(s)$ is a $m \times p$ matrix of functions of s, $\mathbf{x}_i$ is a $p \times 1$ vector of covariates of interest, and $\eta_i(s)$ satisfies $E[\eta_i(s)|\mathbf{x}_i] = 0$ and $\text{Cov}[\eta_i(s), \eta_i(t)|\mathbf{x}_i] = \Gamma_\eta(s, t)$. $B(s)$ characterizes the association between fiber bundle diffusion properties and the covariates of interest $\mathbf{x}_i$.

As an illustration, in our clinical study on early brain development, we are interested in studying the evolution of the three eigenvalues λ_i of diffusion tensor ($\lambda_1 \geq \lambda_2 \geq \lambda_3$) along two selected fiber tracts in 128 healthy pediatric subjects [Fig. 2(a) and Fig. 5(a)]. See clinical data and results section for details. We consider a functional linear model of three eigenvalues along a specific tract as follows:

$$f_{i,1}(s) = (\beta_{11}(s), \beta_{12}(s), \beta_{13}(s), \beta_{14}(s))\mathbf{x}_i + \eta_{i1}(s)$$
$$f_{i,2}(s) = (\beta_{21}(s), \beta_{22}(s), \beta_{23}(s), \beta_{24}(s))\mathbf{x}_i + \eta_{i2}(s)$$
$$f_{i,3}(s) = (\beta_{31}(s), \beta_{32}(s), \beta_{33}(s), \beta_{34}(s))\mathbf{x}_i + \eta_{i3}(s) \quad (14)$$

where $f_{i,k}(\cdot)$ equals the smoothed λ_k curve from the ith subject for $k = 1, 2, 3$, and $\mathbf{x}_i = (1, g_i, \text{Gage}_i, \text{age}_i)^T$, in which g_i and Gage_i denote gender and gestational age, respectively. Moreover, gestational age is the age of a newborn infant, both gestational age and age are continuous covariates, and gender is a discrete covariate. In this case, $m = 3$, $B(s) = (\beta_{jk}(s))$ is a 3×4 matrix, and $\mathbf{x}_i = (1, g_i, \text{Gage}_i, \text{age}_i)^T$.

We develop an estimation algorithm to estimate $B(s)$ and $\Gamma_\eta(s, t)$ as follows.

- Step (2.1) is to estimate $B(s)$. Let $B_k(s)$ be the kth row of $B(s)$. Then, based on the estimated function vectors $\hat{\mathbf{f}}_i(s)$, we calculate the least-squares estimator of $B(s)$, denoted by $\hat{B}(s)$, by minimizing an objective function given by

$$\sum_{i=1}^{n} [\hat{\mathbf{f}}_i(s)^{\text{sec}} - B(s)\mathbf{x}_i]^T [\hat{\mathbf{f}}_i(s)^{\text{sec}} - B(s)\mathbf{x}_i]. \quad (15)$$

Specifically, the least-squares estimator of $B_k(s)$, denoted by $\hat{B}_k(s)$, is given by

$$\hat{B}_k(s)^T = \left(\sum_{i=1}^{n} \mathbf{x}_i^{\otimes 2}\right)^{-1} \sum_{i=1}^{n} \mathbf{x}_i \hat{f}_{i,k}(s)^{\text{sec}} \quad (16)$$

for $k = 1, \ldots, m$.

- Step (2.2) is to estimate $\Gamma_\eta(s,t)$. Let $\hat{\eta}_i(s) = \hat{\mathbf{f}}_i(s)^{\text{sec}} - \hat{B}(s)\mathbf{x}_i$. Then, the covariance matrix $\Gamma_\eta(s,t)$ can be estimated by

$$\hat{\Gamma}_\eta(s,t) = (n-m)^{-1} \sum_{i=1}^{n} \hat{\eta}_i(s)\hat{\eta}_i(t)^T. \quad (17)$$

The covariance matrix $\Gamma_\eta(s,t)$ characterizes the variation of $\eta_i(s)$, which is different from $\Gamma(s,t)$.

To carry out statistical inference on $B(s)$, we need some asymptotic results for $\hat{B}(s)$. Let $\text{vec}(B(s)) = (B_1(s)^T, \ldots, B_m(s)^T)^T$. Theoretically, following the arguments in [36], it can be shown that under some regularity conditions,

$$\sqrt{n}[\text{vec}(\hat{B}(s)) - \text{vec}(B(s)) + O(\hat{h}_{opt}^2)] \to^L \text{GP}(\mathbf{0}, \Gamma_B), \quad (18)$$

where $\to^L$ denotes the convergence in distribution and $\text{GP}(\mathbf{0}, \Gamma_B)$ is a Gaussian process with mean zero and covariance function $\Gamma_B(s,t) = \Gamma_\eta(s,t) \otimes \Omega_X^{-1}$, in which $\otimes$ denotes the Kronecker product of two matrices and $\Omega_X = \lim_{n\to\infty} n^{-1} \sum_{i=1}^{n} \mathbf{x}_i^{\otimes 2}$. The asymptotic result in (18) ensures the validity of constructing the global test statistic detailed below.

D. FRATS: Global Test Statistic

We develop a *global test statistic* to test linear hypotheses of $B(s)$ in order to answer various scientific questions involving a comparison of fiber bundle diffusion properties along fiber bundles across two (or more) diagnostic groups and the development of fiber bundle diffusion properties along time. We can formulate these questions as linear hypotheses of $B(s)$ as follows:

$$H_0 : \mathbf{C}\text{vec}(B(s)) = \mathbf{b}_0(s) \text{ for all } s \quad (19)$$

versus

$$H_1 : \mathbf{C}\text{vec}(B(s)) \neq \mathbf{b}_0(s) \quad (20)$$

where $\mathbf{C}$ is a $r \times mp$ matrix of full row rank and $\mathbf{b}_0(s)$ is a given $r \times 1$ vector of functions.

As an illustration, we are interested in testing the age effect on the evolution of the three eigenvalues of the diffusion tenors along the two selected fiber tracts in 128 healthy pediatric subjects in our clinical study on early brain development. Statistically, for model (1), testing the age effect can be formularized as follows:

$$H_0 : \beta_{14}(s) = \beta_{24}(s) = \beta_{34}(s) = 0 \text{ for all } s$$

versus

$$H_1 : \beta_{14}(s) \neq 0 \text{ or } \beta_{24}(s) \neq 0 \text{ or } \beta_{34}(s) \neq 0.$$

In this case, we have

$$\mathbf{C} = \begin{pmatrix} 0 & 0 & 0 & 1 & 0 & 0 & 0 & 0 & 0 & 0 & 0 & 0 \\ 0 & 0 & 0 & 0 & 0 & 0 & 0 & 1 & 0 & 0 & 0 & 0 \\ 0 & 0 & 0 & 0 & 0 & 0 & 0 & 0 & 0 & 0 & 0 & 1 \end{pmatrix}$$

and $\mathbf{b}_0(s) \equiv (0,0,0)^T$ for all s. The use of multiple diffusion properties in model (13) allows us to compare different functions in $B(s)$ associated with different diffusion properties. For instance, suppose that we want to test

$$H_0 : \beta_{14}(s) = \beta_{24}(s) \text{ for all } s \text{ vs. } H_1 : \beta_{14}(s) \neq \beta_{24}(s).$$

In this case, we have

$$\mathbf{C} = (0 \quad 0 \quad 0 \quad 1 \quad 0 \quad 0 \quad 0 \quad -1 \quad 0 \quad 0 \quad 0 \quad 0)$$

and $\mathbf{b}_0(s) \equiv (0)$ for all s.

We test the null hypothesis $H_0 : \mathbf{C}\text{vec}(B(s)) = \mathbf{b}_0(s)$ using a global test statistic S_n defined by

$$S_n = n \int_0^{F_0} \mathbf{d}(s)^T [\mathbf{C}(\hat{\Gamma}_\eta(s,s) \otimes \hat{\Omega}_X^{-1})\mathbf{C}^T]^{-1} \mathbf{d}(s) ds, \quad (21)$$

where $\hat{\Omega}_X = n^{-1} \sum_{i=1}^{n} \mathbf{x}_i^{\otimes 2}$, $\mathbf{d}(s) = \mathbf{C}\text{vec}(\hat{B}(s)) - \mathbf{b}_0(s)$, and F_0 is the whole arc length of a specific fiber bundle. In order to use S_n as a test statistic, we need an asymptotic result. Specifically, similar to the arguments in [36], we can show that under some conditions and H_0, $\sqrt{n}\mathbf{d}(s)$ and S_n converge weakly to $N(\mathbf{0}, \mathbf{C}(\Gamma_\eta(s,s) \otimes \Omega_X^{-1})\mathbf{C}^T)$ and a weighted χ^2 distribution, respectively, as $n \to \infty$.

In addition, at a given grid point s_j on a specific tract, we can also test the local null hypothesis $H_0(s_j) : \mathbf{C}\text{vec}(B(s_j)) = \mathbf{b}_0(s_j)$ using a local test statistic $S_n(s_j)$ defined by

$$S_n(s_j) = n\mathbf{d}(s_j)^T [\mathbf{C}(\hat{\Gamma}_\eta(s_j,s_j) \otimes \hat{\Omega}_X^{-1})\mathbf{C}^T]^{-1} \mathbf{d}(s_j). \quad (22)$$

Under some conditions and $H_0(s_j)$, $\sqrt{n}\mathbf{d}(s_j)$ and $S_n(s_j)$ converge weakly to $N(\mathbf{0}, \mathbf{C}(\Gamma_\eta(s_j,s_j) \otimes \Omega_X^{-1})\mathbf{C}^T)$ and a weighted χ^2 distribution with r degrees of freedom, respectively, as $n \to \infty$.

E. FRATS: Resampling Method

We develop a *resampling method* (or wild bootstrap method) to approximate the *p*-value of S_n [37], [38]. The resampling method has four key steps as follows.

- Step (3.1): Fit the functional linear model $\hat{\mathbf{f}}_i(s) = B(s)\mathbf{x}_i + \eta_i(s)$, $i = 1, \ldots, n$, under the null hypothesis H_0, which yields $\hat{B}^*(s)$ and $\hat{\eta}_i^*(s) = \hat{\mathbf{f}}_i(s) - \hat{B}^*(s)\mathbf{x}_i$.
- Step (3.2): Generate a random sample $\tau_i^{(g)}$ from a $N(0,1)$ generator for $i = 1, \ldots, n$ and then construct $\hat{\mathbf{f}}_i(s)^{(g)} = \hat{B}^*(s)\mathbf{x}_i + \tau_i^{(g)}\hat{\eta}_i^*(s)$. Then, based on $\hat{\mathbf{f}}_i(s)^{(g)}$, we calculate

$$\hat{B}_k(s)^{(g)T} = \left(\sum_{i=1}^{n} \mathbf{x}_i^{\otimes 2}\right)^{-1} \sum_{i=1}^{n} \mathbf{x}_i \hat{f}_{i,k}(s)^{(g)} \quad (23)$$

for $k = 1, \ldots, m$, where $\hat{B}_k(s)^{(g)T}$ and $\hat{f}_{i,k}(s)^{(g)}$ are, respectively, the kth row of $\hat{B}(s)^{(g)}$ and $\hat{\mathbf{f}}_i(s)^{(g)}$. Finally, let $\mathbf{d}(s)^{(g)} = \mathbf{C}\text{vec}(\hat{B}(s)^{(g)}) - \mathbf{b}_0(s)$, we compute $S_n^{(g)} = n \int_0^{F_0} \mathbf{d}(s)^{(g)T}[\mathbf{C}(\hat{\Gamma}_\eta(s,s) \otimes \hat{\Omega}_X^{-1})\mathbf{C}^T]^{-1}\mathbf{d}(s)^{(g)}ds$
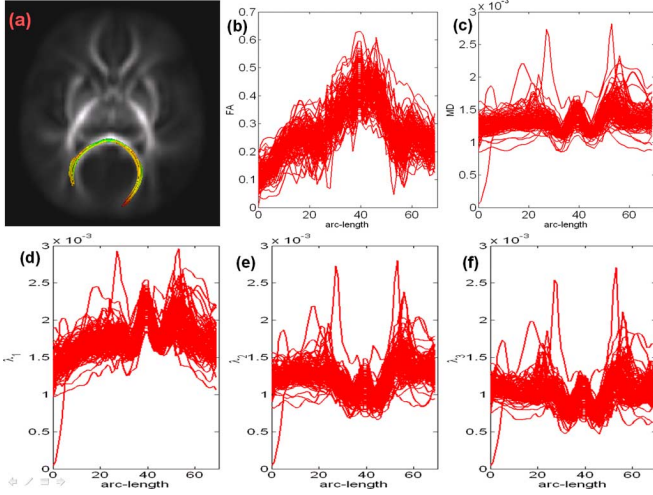
Fig. 2.   Splenium tract and diffusion properties along the splenium tract: (a) the splenium tract extracted from the tensor atlas with color representing mean FA value; (b) FA; (c) MD; (d) λ_1; (e) λ_2; (f) λ_3. The diffusion properties in (b)–(f) are sampled along the atlas-normalized arc length for all 128 subjects.
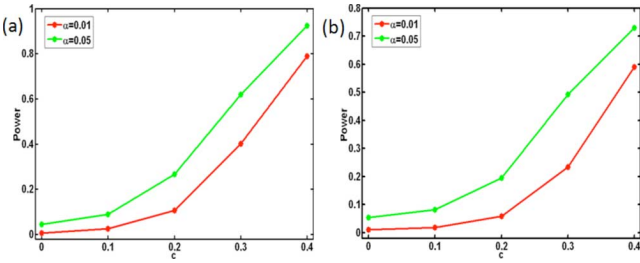

Fig. 3.   Simulation study: Type I and Type II error rates. Rejection rates of S_n based on the resampling method are calculated at five different values of c for sample sizes of 64, 128 subjects at the 5% (green) and 1% (red) significance levels: (a) $n = 128$; (b) $n = 64$.
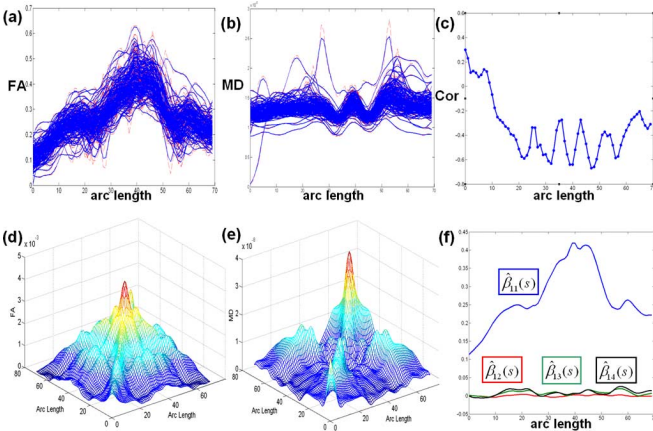

Fig. 4.   Results from the analysis of FA and MD on the splenium tract: reconstructed curves $\hat{\mathbf{f}}_i(s)^{\text{sec}}$ for FA in panel (a) and MD in panel (b); (c) estimated correlation between FA and MD along the tract; estimated covariance matrices $\hat{\Gamma}(s,t)$ for FA in panel (d) and MD in panel (e); (f) estimated regression coefficient functions for FA: $\hat{\beta}_{11}(s)$ for intercept (blue), $\hat{\beta}_{12}(s)$ for gender (red), $\hat{\beta}_{13}(s)$ for gestational age (green), and $\hat{\beta}_{14}(s)$ for age (black).
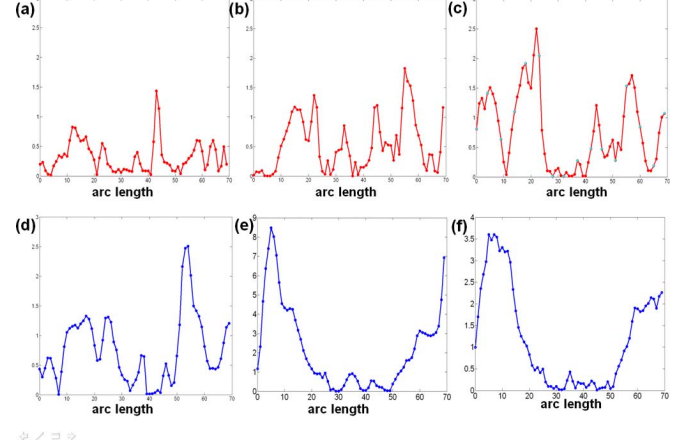

Fig. 5.   Results from the analysis of FA and MD on the splenium tract: the $-\log_{10}(p)$ values of test statistics $S_n(s_j)$ for testing gender effect in panel (a), gestational age effect in panel (b), and age effect in panel (c) on FA; the $-\log_{10}(p)$ values of test statistics $S_n(s_j)$ for testing gender effect in panel (d), gestational age effect in panel (e), and age effect in panel (f) on MD.

- Step (3.3): Repeat Step (3.2) G times to obtain $\{S_{n,\max}^{(g)} = \max_{1 \le j \le L_0} S_n(s_j)^{(g)} : g = 1, \ldots, G\}$ and calculate

$$p(s_j) = G^{-1} \sum_{g=1}^{G} 1(S_{n,\max}^{(g)} \ge S_n(s_j))$$

  for each s_j. The $p(s_j)$ is the corrected p-value at the location s_j.

- Step (3.4): Repeat Step (3.2) G times to obtain $\{S_n^{(g)} : g = 1, \ldots, G\}$ and calculate

$$p = G^{-1} \sum_{g=1}^{G} 1(S_n^{(g)} \ge S_n).$$

If p is smaller than a pre-specified value α, say 0.05, then we reject the null hypothesis H_0.

We note several advantages of using the resampling method in the above test procedure. Computationally, the above procedure only requires the repeated calculation of $\hat{B}_k^{(g)}$ and $S_n^{(g)}$. Thus, because computing $\hat{B}_k^{(g)}$ is very fast, the proposed test procedure is computationally efficient. The proposed resampling method also performs better than parametric bootstrap. Specifically, the parametric bootstrap requires parametric assumptions for $\eta_i(s)$. Moreover, for functional linear model (13), permutation method is not directly applicable without very strong assumption such as complete exchangeability.

F. Monte Carlo Simulations

We conducted a set of Monte Carlo simulations to evaluate the Type I and II error rates of the global test statistic S_n based on the resampling method. We simulated FA and MD measures along the right internal capsule tract [Fig. 7(a)] obtained from our clinical data according to

$$(\text{FA}_i(s_j), \text{MD}_i(s_j))^T$$
$$= (f_{i,1}(s_j), f_{i,2}(s_j))^T + \epsilon_{i,j}$$
$$f_{i,1}(s) = (\beta_{11}(s), \beta_{12}(s), \beta_{13}(s), \beta_{14}(s))\mathbf{x}_i + \eta_{i1}(s)$$
$$f_{i,2}(s) = (\beta_{21}(s), \beta_{22}(s), \beta_{23}(s), \beta_{24}(s))\mathbf{x}_i + \eta_{i2}(s)$$

and $S_n(s_j)^{(g)} = n\mathbf{d}(s_j)^{(g)T}[\mathbf{C}(\hat{\Gamma}_\eta(s_j, s_j) \otimes \hat{\Omega}_X^{-1})\mathbf{C}^T]^{-1}\mathbf{d}(s_j)^{(g)}$ for $j = 1, \ldots, L_0$.
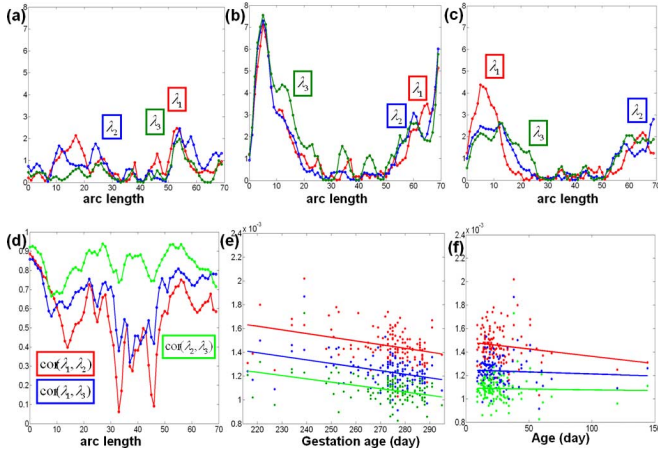
Fig. 6. Results from the analysis of the three eigenvalues of diffusion tensor on the splenium tract: the $-\log_{10}(p)$ values of test statistics $S_n(s_j)$ for testing gender effect in panel (a), gestational age effect in panel (b), and age effect in panel (c) on λ_1 (red), λ_2 (blue) and λ_3 (green); correlations among λ_1, λ_2 and λ_3 in panel (d); scatter plots of λ_1 (red), λ_2 (blue), and λ_3 (green) against gestational age and age in panels (e) and (f), respectively.
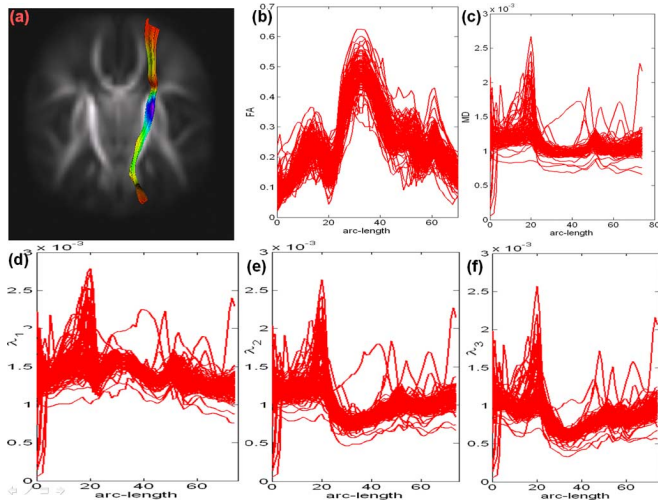

Fig. 7. Right internal capsule tract and diffusion properties along the tract: (a) the right internal capsule tract extracted from the tensor atlas with color representing mean FA value; (b) FA; (c) MD; (d) λ_1; (e) λ_2; (f) λ_3. The diffusion properties in panels (b)–(f) are sampled along the atlas-normalized arc length for all 128 subjects.

where $\mathbf{x}_i = (1, g_i, \text{Gage}_i, \text{age}_i)^T$, $\eta_i(s) = (\eta_{i1}(s), \eta_{i2}(s))^T$ is a 2×1 vector of Gaussian process with zero mean and covariance matrix $\Gamma_\eta(s, t)$ and $\epsilon_{i,j}$ is a 2×1 vector of Gaussian random variables with zero mean and covariance matrix $\Sigma(s_j)$. To mimic imaging data in practice, we used FA and MD measures along the right internal capsule tract from the 128 subjects in our clinical data to estimate $\hat{\Sigma}(s_j)$ of $\Sigma(s_j)$ via (7), $\hat{B}(s)$ of $B(s)$ via (16), and $\hat{\Gamma}_\eta(s, t)$ via (17). Then, except for $(\beta_{12}(s), \beta_{22}(s))$ for all s, we fixed all other parameters at their values obtained from our clinical data, whereas we assumed $(\beta_{12}(s), \beta_{22}(s)) = c(\hat{\beta}_{12}(s), \hat{\beta}_{22}(s))$, where c is a scalar specified below and $(\hat{\beta}_{12}(s), \hat{\beta}_{22}(s))$ were estimators obtained from our clinical data.

We tested the hypotheses $H_0 : \beta_{12}(s) = \beta_{22}(s) = 0$ for all s along the right internal capsule tract against $H_1 : \beta_{12}(s) \neq 0$

or $\beta_{22}(s) \neq 0$ for at least a s on the tract. We assumed $c = 0$ to assess the Type I error rates for the global test statistic, and then we assumed $c = 0.1, 0.2, 0.3$, and 0.4 to examine the Type II error rates for S_n. In both cases,

$$\mathbf{C} = \begin{pmatrix} 0 & 1 & 0 & 0 & 0 & 0 & 0 & 0 \\ 0 & 0 & 0 & 0 & 0 & 1 & 0 & 0 \end{pmatrix} \text{ and } \mathbf{b}_0(s) \equiv \begin{pmatrix} 0 \\ 0 \end{pmatrix}$$

for all s. We set $n = 128$ and 64. For $n = 128$, we used the same values of age, gestational age, and gender from all 128 subjects in our clinical data. For $n = 64$, we randomly chose 32 males and 32 females from our clinical data and used their values of age, gestational age, and gender to simulate the values of FA and MD along the right internal capsule tract.

For each simulation, the significance levels were set at $\alpha = 5\%$ and 1%, and 1,000 replications were used to estimate the rejection rates. For a fixed α, if the Type I rejection rate is smaller than α, then the test is conservative, whereas if the Type I rejection rate is greater than α, then the test is anticonservative, or liberal.

G. Clinical Data

This study was approved by the Institute Review Board of the University of North Carolina at Chapel Hill. A total of 128 healthy full-term subjects (75 M and 53 F) during the first year of age were recruited and written informed consent was obtained from their parents before imaging acquisition. The subjects were taken from a larger study designated to investigating early brain development at our institution. A total of 128 neonates with a mean postnatal age of 25 ± 17.9 days (range: 9–144 days) were included in this study. Efforts were made to ensure the subjects slept comfortably inside the MR scanner, and thus none of the subjects was sedated during imaging session. All subjects were fed and calmed to sleep on a warm blanket with proper ear protection.

All images were acquired on a 3 T Allegra head only MR system (Siemens Medical Inc., Erlangen, Germany) with a maximal gradient strength of 40 mT/m and a maximal slew rate of 400 mT/(m $\cdot$ ms). A single shot EPI DTI sequence (TR/TE = 5400/73 ms) with eddy current compensation was used to obtain DTI images. Diffusion gradients with a b-value of 1000 s/mm^2 were applied in six noncollinear directions, $(1,0,1)$, $(-1,0,1)$, $(0,1,1)$, $(0,1,-1)$, $(1,1,0)$, and $(-1,1,0)$. The reference scan $(b = 0)$ was also acquired for the construction of diffusion tensor matrices. Contiguous slices with slice thickness of 2 mm were scanned to cover the whole brain. The voxel resolution was isotropic 2 mm, and the in-plane field of view was 256 mm in both directions. A total of five scans were acquired and averaged to improve the signal-to-noise ratio of the images.

A weighted least square estimation method was used to construct the diffusion tensors [2], [27]. Then the image processing steps in the DTI atlas building were used to process all 128 DTI data sets and compute diffusion properties along all fiber tracts of interest. For the sake of space, we chose two tracts of interest including the splenium of the corpus callosum tract and the right internal capsule tract (Figs. 2(a) and 7(a)) and then computed fractional anistropy (FA), mean diffusivity (MD), and the three eigenvalues of the diffusion tensors, denoted by $\lambda_1 \geq \lambda_2 \geq \lambda_3$,

at each grid point on both tracts for each of the 128 subjects. FA denotes the inhomogeneous extent of local barriers to water diffusion, while MD measures the averaged magnitude of local water diffusion. The three eigenvalues of diffusion tensor may, respectively, reflect the magnitude of water diffusivity along and perpendicular to the long axis of white matter fibers [39].

We applied FRATS to the joint analysis of FA and MD values along the splenium tract as follows. We fitted the functional linear model (13) to these smoothed FA and MD functions from all 128 subjects, in which $\mathbf{x}_i = (1, g_i, \mathrm{Gage}_i, \mathrm{age}_i)^T$ and $m = 2$, and then we used (16) to estimate the function of regression coefficient vector $\hat{B}(s)$. Secondly, we constructed the global test statistic S_n to test the effects of all the three covariates for FA alone, MD alone, and joint FA and MD, respectively, and performed hypothesis testing on the whole splenium tract. The p-value of S_n was approximated using the resampling method with $G = 10,000$. Based on the significant results for MD, we further analyzed the three eigenvalues of diffusion tensors along the splenium tract using the same steps.

Similar to the analysis of the splenium tract, we also applied FRAST to the analysis of FA and MD values along the right internal capsule tract. Then, we fitted the functional linear model (13) to these smoothed FA and MD functions from all 128 subjects, in which $\mathbf{x}_i = (1, g_i, \mathrm{Gage}_i, \mathrm{age}_i)^T$ and $m = 2$. We performed formal hypothesis testings in order to examine the effects of gender, gestational age, and age on FA and MD values along the right internal capsule tract. We further analyzed the three eigenvalues of diffusion tensors along the right internal capsule tract.

III. RESULTS

A. Monte Carlo Simulations

Overall, the rejection rates for S_n based on the resampling method were accurate for all sample sizes ($n = 64$, or 128) at both significance levels ($\alpha = 0.01$ or 0.05) [Fig. 3(a) and (b)]. Consistent with our expectations, the statistical power for rejecting the null hypothesis increased with the sample size.

B. Clinical Data: Splenium Tract

We used the adaptive local polynomial kernel smoothing technique to simultaneously smooth FA and MD function vectors for each of 128 subjects, which leads to the smoothed curves [Fig. 4(a) and (b)]. We computed the sample covariance matrix and obtained correlation coefficient between FA and MD at each grid point. We observed negative correlations at most grid points [Fig. 4(c)]. Based on the smoothed FA and MD functions, we estimated their mean functions and their covariance functions using (11) and (12) [Fig. 4(d) and (e)]. Then, we fitted the functional linear model (13) to the smoothed FA and MD functions from all 128 subjects, in which $\mathbf{x}_i = (1, g_i, \mathrm{Gage}_i, \mathrm{age}_i)^T$ and $m = 2$. The elements of $\hat{B}(s)$ corresponding to FA are shown in Fig. 4(f).

From our model, we performed formal hypothesis testings in order to examine the effects of gender, gestational age, and age on FA and MD values along the splenium tract. We first considered tests based on FA and MD, respectively, and performed hypothesis testing at each grid point along the splenium tract

TABLE I
p-VALUES OF S_n FOR TESTING THE EFFECTS OF GENDER, GESTATIONAL AGE (GAGE), AND AGE ON THE SPLENIUM AND RIGHT INTERNAL CAPSULE TRACTS

	Splenium			Right internal capsule		
	gender	Gage	age	gender	Gage	age
FA	0.994	0.650	0.404	0.664	0.012	0.001
MD	0.196	0.002	0.072	0.790	$< 10^{-4}$	$< 10^{-4}$
(FA, MD)	0.111	0.004	0.038	0.245	$< 10^{-4}$	$< 10^{-4}$
λ_1	0.212	0.006	0.105	0.821	0.0001	0.022
λ_2	0.169	0.005	0.142	0.747	$< 10^{-4}$	$< 10^{-4}$
λ_3	0.594	0.011	0.101	0.753	$< 10^{-4}$	$< 10^{-4}$
$(\lambda_1, \lambda_2, \lambda_3)$	0.063	0.004	0.061	0.298	$< 10^{-4}$	$< 10^{-4}$

(Fig. 5). For FA alone, no significant effect of any covariate was found, even though the $-\log_{10}(p)$ value of $S_n(s)$ for age at a single grid point was slightly greater than 2 [Fig. 5(c)]. For MD alone, no significant gender effect was found [Fig. 5(d)], whereas the effects of age and gestational age were significant at the head and tail of the splenium tract [Fig. 5(e) and (f)].

For FA alone, no significant effects of all covariates were found in Table I, which agrees with our previous findings based on the local test statistics $S_n(s)$. This indicates that the degree of anisotropy on the splenium tract does not differ significantly between male and female groups and does not change significantly with gestational age and age. For MD alone, we observed a significant association between gestational age and MD and a marginal significance for age. This indicates a significant change of the degrees of diffusivity, not the degree of anisotropy, along the splenium tract. For joint FA and MD on the splenium tract, no significant gender effect was found, whereas the effects of both age and gestational age were significant.

Along the splenium tract, we observed positive correlations among the three eigenvalues [Fig. 6(d)]. Particularly, large correlations between λ_2 and λ_3 along the splenium tract indicate the small differences between λ_2 and λ_3 on the splenium tract [Fig. 2(e) and (f)], whereas relatively weak correlations between λ_1 and λ_3 indicate large differences between λ_1 and λ_3 along the splenium tract [Fig. 2(d)]. Then, we fitted the functional linear model (13) to the smoothed three eigenvalues functions from all 128 subjects, in which $\mathbf{x}_i = (1, g_i, \mathrm{Gage}_i, \mathrm{age}_i)^T$ and $m = 3$.

We examined association between all covariates of interest and all eigenvalues along the splenium tract by performing formal hypothesis testing at each grid point. No significant gender effect was found for all the three eigenvalues [Fig. 6(a)], whereas significant gestational age effect was observed at the head and tail of the splenium tract [Fig. 6(b)]. We observed a similar association pattern between gestational age and the three eigenvalues of DT [Fig. 6(b)]. We picked a grid point with a significant p value of $S_n(s)$ and observed that the three eigenvalues decrease with gestational age. For age, a similar association pattern was observed for λ_2 and λ_3, whereas λ_1 was significantly associated with age at the head of the splenium tract [Fig. 6(c)].

C. Clinical Data: Right Internal Capsule Tract

We simultaneously smoothed the FA and MD function vectors of all 128 subjects and then estimated their mean functions [Fig. 8(a) and (d)] and their covariance functions [Fig. 8(b) and (e)]. Then, we fitted the functional linear model
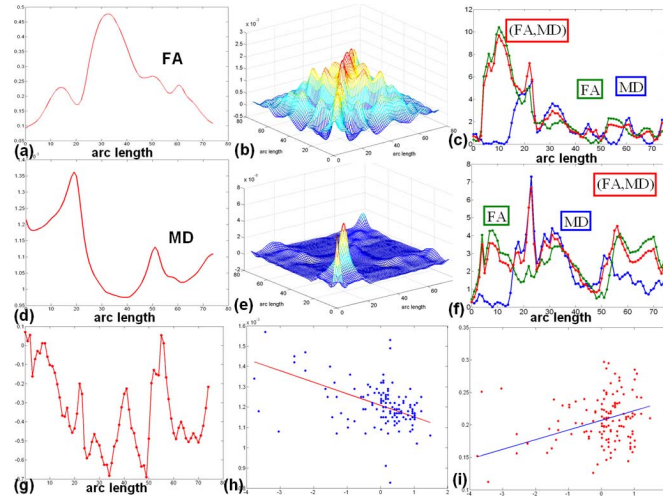
Fig. 8. Results obtained from the analysis of FA and MD on the right internal capsule tract: the estimated mean function and covariance function for FA in panels (a) and (b), respectively; the estimated mean function and covariance function for MD in panels (d) and (e), respectively; (g) the correlation between FA and MD; the $-\log_{10}(p)$ values of test statistics $S_n(s_j)$ for testing gestational age and age effect on FA (green), MD (blue), and (FA, MD) (red) in panels (c) and (f), respectively; scatter plots of MD and FA measures from a selected grid point against standardized gestational age, abbreviated as S-gestation age, in panels (h) and (i), respectively.
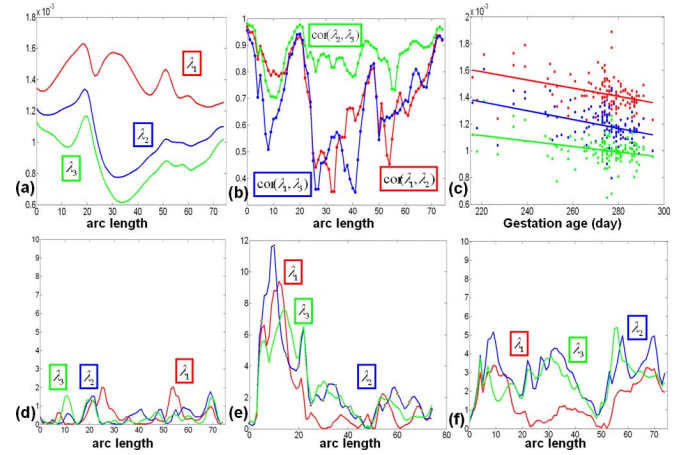

Fig. 9. Results from the analysis of the three eigenvalues of diffusion tensor on the right internal capsule tract: (a) the estimated mean functions for λ_1 (red), λ_2 (blue), and λ_3 (blue); (b) correlations among λ_1, λ_2, and λ_3; (c) scatter plot of λ_1 (red), λ_2 (blue), and λ_3 (green) from a selected grid point against gestational age; the $-\log_{10}(p)$ values of test statistics $S_n(s_j)$ for testing gender effect in panel (d), gestational age effect in panel (e), and age effect in panel (f) on λ_1 (red), λ_2 (blue), and λ_3 (green).

(13) to the smoothed FA and MD functions from all 128 subjects, in which $\mathbf{x}_i = (1, \mathrm{g}_i, \mathrm{Gage}_i, \mathrm{age}_i)^T$ and $m = 2$. We considered tests based on FA alone, MD alone, and (FA, MD), respectively, and performed hypothesis testing at each grid point along the right internal capsule tract [Fig. 8(c) and (f)]. No significant gender effect was found for all tests (Table I). For FA alone, significant gestational age and age effects were observed for the right internal capsule tract [Fig. 8(c) and (f)]. We observed negative correlations between FA and MD at most grid points [Fig. 8(g)]. We picked a grid point with the significant p value of $S_n(s)$ at the significance level 5% and observed the increasing pattern of FA with the standardized gestational age [Fig. 8(i)]. For MD alone, significant gestational age and age effects were found in the middle of the right internal capsule tract [Fig. 8(f)]. We picked a grid point with the significant p value of $S_n(s)$ and observed the decreasing pattern of MD with the standardized gestational age [Fig. 8(h)].

We also constructed the global test statistic S_n to assess the covariates of interest based on FA alone, MD alone, and (FA, MD), respectively, and performed hypothesis testing on the right internal capsule tract. The p-value of S_n was approximated using the resampling method with $G = 10\,000$. The resulting p-values are reported in Table I. No significant gender effect was found for all scenarios, which indicates no significant difference between male and female groups. We observed significant gestational age and age effects for both FA and MD. Our results agree with previous DTI findings. Current DTI studies including neonates have revealed that FA and MD respectively increases and decreases with age. In white matter, neonates have significantly lower anisotropy values and significantly higher MD values compared to adults [40], [41].

We also observed positive correlations among the three eigenvalues [Fig. 9(b)]. We observed large correlation between λ_2

and λ_3 and relatively weak correlation between λ_1 and λ_3. This agrees with the small differences between λ_2 and λ_3 along the right internal capsule tract [Fig. 7(d)–(f)] and the relatively large differences between λ_1 and λ_3 in the middle of the right internal capsule tract [Fig. 7(d)–(f)]. Then, we fitted the functional linear model (13) to the smoothed three eigenvalues functions from all 128 subjects, in which $\mathbf{x}_i = (1, \mathrm{g}_i, \mathrm{Gage}_i, \mathrm{age}_i)^T$ and $m = 3$. We performed formal hypothesis testings by examining the association between all covariates of interest and the three eigenvalues along the right internal capsule tract at each grid point. No significant gender effect was found for all the three eigenvalues [Fig. 9(d)]. Gestational age was strongly associated with all the three eigenvalues [Fig. 9(e)]. The scatter plot at a selected grid point shows the decreasing pattern for all eigenvalues with the gestational age. We observed a moderate age effect on all the three eigenvalues [Fig. 9(f)].

IV. CONCLUSION AND DISCUSSION

The contributions of our work are two folds. Technically, we have presented a novel functional regression framework, called FRATS, for analyzing multiple fiber bundle diffusion properties with a set of covariates of interest, such as age, diagnostic status and gender, in real applications. FRATS can be used to understand normal brain development, the neural bases of neuropsychiatric disorders, and the joint effects of environmental and genetic factors on white matter fiber bundles. From the application end, FRATS is applied to characterizing the development of diffusion properties on fiber bundles in a clinical study of neurodevelopment. Our approach is able to reveal the complex inhomogeneous spatiotemporal maturation patterns as the apparent changes in FA, MD, and the three eigenvalues of DT. Specifically, our results suggest that white matter maturation patterns are different in different white matter regions.

There are still limitations that need to be addressed. First, we have focused on the analysis of a set of water diffusion related parameters based on diffusion tensor image rather than those

based on high angular resolution diffusion image (HARDI), because diffusion tensor image is commonly used for characterizing major white matter fiber bundles. In the future, we will apply FRATS to water diffusion related parameters obtained from HARDI [42]–[44]. Second, we have focused on tensor derived univariate measures. It is also interesting to extend FRATS to principal directions and full diffusion tensors on fiber bundles [45]–[49]. Third, we have focused on analyzing fiber bundle diffusion properties with a set of covariates. The proposed methodology can be readily extended to more complex fiber structures, such as the medial manifolds of fiber tracts [25]. Fourth, we have focused on cross-sectional studies. Extending FRATS to longitudinal studies and family studies requires further research [50].

We have developed FRATS for statistically analyzing multiple diffusion properties along fiber bundle and assessing their association with a set of covariates of interest in real applications. FRATS integrates four statistical tools for formally testing hypothesis of interest and carrying out statistical inference in real applications. The proposed methodology is demonstrated in a clinical study of neurodevelopment. In this study, significant age and gestational age effects on multiple diffusion properties were examined and localized in two representative tracts. We expect that this novel statistical tool will lead to new findings in our clinical applications.

ACKNOWLEDGMENT

REFERENCES

[1] P. J. Basser, J. Mattiello, and D. LeBihan, "MR diffusion tensor spectroscopy and imaging," *Biophys. J.*, vol. 66, pp. 259–267, 1994.

[2] P. J. Basser, J. Mattiello, and D. LeBihan, "Estimation of the effective self- diffusion tensor from the NMR spin echo," *J. Magn. Reson. Ser. B*, vol. 103, pp. 247–254, 1994.

[3] C. Pierpaoli and P. J. Basser, "Toward a quantitative assessment of diffusion anisotropy," *Magn. Reson. Med.*, vol. 36, pp. 893–906, 1996.

[4] K. M. Hasan, P. J. Basser, D. L. Parker, and A. L. Alexander, "Analytical computation of the eigenvalues and eigenvectors in DT-MRI," *J. Magn. Reson.*, vol. 152, pp. 41–47, 2001.

[5] K. M. Hasan and P. A. Narayana, "Computation of the fractional anisotropy and mean diffusivity maps without tensor decoding and diagonalization: Theoretical analysis and validation," *Magn. Reson. Med.*, vol. 50, pp. 589–598, 2003.

[6] H. T. Zhu, D. Xu, R. Amir, X. Hao, H. Zhang, K. Alayar, B. Ravi, and B. Peterson, "A statistical framework for the classification of tensor morphologies in diffusion tensor images," *Magn. Reson. Imag.*, vol. 24, pp. 569–582, 2006.

[7] M. Moseley, "Diffusion tensor imaging and aging—A review," *NMR Biomed.*, vol. 15, pp. 553–560, 2002.

[8] P. Mukherjee and R. C. McKinstry, "Diffusion tensor imaging and tractography of human brain development," *Neuroimag. Clin. N. Am.*, vol. 16, pp. 19–43, 2006.

[9] C. J. Cascio, G. Gerig, and J. Piven, "Diffusion tensor imaging: Application to the study of the developing brain," *J. Am. Acad. Child Adolescent Psychiatry*, vol. 46, pp. 213–223, 2007.

[10] N. K. Rollins, "Clinical applications of diffusion tensor imaging and tractography in children," *Pediatric Radiol.*, vol. 37, pp. 769–780, 2007.

[11] S. M. Smith, M. Jenkinson, H. Johansen-Berg, D. Rueckert, T. E. Nichols, C. E. Mackay, K. E. Watkins, O. Ciccarelli, M. Z. Cader, P. M. Matthews, and T. E. Behrens, "Tractbased spatial statistics: Voxelwise analysis of multi-subject diffusion data," *NeuroImage*, vol. 31, pp. 1487–1505, 2006.

[12] L. J. O'Donell, C. F. Westin, and A. J. Golby, "Tract-based morphometry for white matter group analysis," *NeuroImage*, vol. 45, pp. 832–844, 2009.

[13] L. Snook, C. Plewes, and C. Beaulieu, "Voxel based versus region of interest analysis in diffusion tensor imaging of neurodevelopment," *NeuroImage*, vol. 34, pp. 243–252, 2007.

[14] D. Bonekamp, L. M. Nagae, M. Degaonkar, M. Matson, W. M. A. Abdalla, P. B. Barker, S. Mori, and A. Horská, "Diffusion tensor imaging in children and adolescents: Reproducibility, hemispheric, and age-related differences," *NeuroImage*, vol. 34, pp. 733–742, 2008.

[15] J. H. Gilmore, L. C. Smith, H. M. Wolfe, B. S. Hertzberg, J. K. Smith, N. C. Chescheir, D. D. Evans, C. Kang, R. M. Hamer, W. Lin, and G. Gerig, "Prenatal mild ventriculomegaly predicts abnormal development of the neonatal brain," *Biol. Psychiatry*, vol. 64, pp. 1069–1076, 2008.

[16] Y. S. Chen, H. Y. An, H. T. Zhu, T. Stone, J. K. Smith, C. Hall, E. Bullitt, D. G. Shen, and W. L. Lin, "White matter abnormalities revealed by diffusion tensor imaging in non-demented and demented HIV+ patients," *NeuroImage*, vol. 47, pp. 1154–1162, 2009.

[17] N. K. Focke, M. Yogarajah, S. B. Bonelli, P. A. Bartlett, M. R. Symms, and J. S. Duncan, "Voxel-based diffusion tensor imaging in patients with mesial temporal lobe epilepsy and hippocampal sclerosis," *NeuroImage*, vol. 40, pp. 728–737, 2008.

[18] E. Càmara, N. Bodammer, A. Rodríguez-Fornells, and C. Tempelmann, "Age-related water diffusion changes in human brain: A voxel-based approach," *NeuroImage*, vol. 34, pp. 1588–1599, 2007.

[19] L. Snook, L. A. Paulson, D. Roy, L. Phillips, and C. Beaulieu, "Diffusion tensor imaging of neurodevelopment in children and young adults," *NeuroImage*, vol. 26, pp. 1164–1173, 2005.

[20] J. Ashburner and K. J. Friston, "Voxel-based morphometry: The methods," *NeuroImage*, vol. 11, pp. 805–821, 2000.

[21] T. D. Wager, M. C. Keller, S. C. Lacey, and J. Jonides, "Increased sensitivity in neuroimaging analyses using robust regression," *Neuroimage*, vol. 26, pp. 99–113, 2005.

[22] K. J. Worsley, J. E. Taylor, F. Tomaiuolo, and J. Lerch, "Unified univariate and multivariate random field theory," *NeuroImage*, vol. 23, pp. 189–195, 2004.

[23] W. V. Hecke, J. Sijbers, S. D. Backer, D. Poot, P. M. Parizel, and A. Leemans, "On the construction of a ground truth framework for evaluating voxel-based diffusion tensor mri analysis methods," *NeuroImage*, vol. 46, pp. 692–707, 2009.

[24] D. K. Jones, M. R. Symms, M. Cercignani, and R. J. Howard, "The effect of filter size on VBM analyses of DT-MRI data," *NeuroImage*, vol. 26, pp. 546–554, 2005.

[25] P. A. Yushkevich, H. Zhang, T. J. Simon, and J. C. Gee, "Structure-specific statistical mapping of white matter tracts," *Neuroimage*, vol. 41, pp. 448–461, 2008.

[26] C. B. Goodlett, P. T. Fletcher, J. H. Gilmore, and G. Gerig, "Group analysis of dti fiber tract statistics with application to neurodevelopment," *NeuroImage*, vol. 45, pp. S133–S142, 2009.

[27] H. T. Zhu, H. P. Zhang, J. G. Ibrahim, and B. G. Peterson, "Statistical analysis of diffusion tensors in diffusion-weighted magnetic resonance image data (with discussion)," *J. Am. Stat. Assoc.*, vol. 102, pp. 1085–1102, 2007.

[28] S. Joshi, B. Davis, M. Jomier, and G. Gerig, "Unbiased diffeomorphic atlas construction for computational anatomy," *Neuroimage*, vol. 23, pp. S151–S160, 2004.

[29] D. C. Alexander, C. Pierpaoli, P. J. Basser, and J. C. Gee, "Spatial transformations of diffusion tensor magnetic resonance images," *IEEE Trans. Med. Imag.*, vol. 20, no. 11, pp. 1131–1139, Nov. 2001.

[30] V. Arsigny, P. Fillard, X. Pennec, and N. Ayache, "Log-euclidean metrics for fast and simple calculus on diffusion tensors," *Magn. Reson. Med.*, vol. 56, pp. 411–421, 2006.

[31] J. Fan and I. Gijbels, *Local Polynomial Modelling and Its Applications*. London, U.K.: Chapman and Hall, 1996.

[32] M. P. Wand and M. C. Jones, *Kernel Smoothing*. London, U.K.: Chapman and Hall, 1995.

[33] H. L. Wu and J. T. Zhang, *Nonparametric Regression Methods for Longitudinal Data Analysis*. Hoboken, NJ: Wiley, 2006.

[34] J. O. Ramsay and B. W. Silverman, *Functional Data Analysis*. New York: Springer-Verlag, 2005.

[35] A. H. Welsh and T. W. Yee, "Local regression for vector responses," *J. Stat. Plann. Inference*, vol. 136, pp. 3007–3031, 2006.

[36] J. Zhang and J. Chen, "Statistical inference for functional data," *Ann. Stat.*, vol. 35, pp. 1052–1079, 2007.

[37] H. T. Zhu, J. G. Ibrahim, N. Tang, D. B. Rowe, X. Hao, R. Bansal, and B. S. Peterson, "A statistical analysis of brain morphology using wild bootstrapping," *IEEE Trans. Med. Imag.*, vol. 26, no. 7, pp. 954–966, Jul. 2007.

[38] D. Y. Lin, "An efficient Monte Carlo approach to assessing statistical significance in genomic studies," *Bioinformatics*, vol. 6, pp. 781–787, 2005.

[39] S. K. Song, S. W. Sun, W. K. Ju, S. J. Lin, A. H. Cross, and A. H. Neufeld, "Diffusion tensor imaging detects and differentiates axon and myelin degeneration in mouse optic nerve after retinal ischemia," *Neuroimage*, vol. 20, pp. 1714–1722, 2003.

[40] J. J. Neil, S. I. Shiran, R. C. McKinstry, G. L. Schefft, A. Z. Snyder, C. R. Almli, E. Akbudak, J. A. Aronovitz, J. P. Miller, B. C. Lee, and T. E. Conturo, "Normal brain in human newborns: Apparent diffusion coefficient and diffusion anisotropy measured by using diffusion tensor mr imaging," *Radiology*, vol. 209, pp. 57–66, 1998.

[41] G. Zhai, W. Lin, K. P. Wilber, G. Gerig, and J. H. Gilmore, "Comparisons of regional white matter diffusion in healthy neonates and adults performed with a 3.0-T head-only MR imaging unit," *Radiology*, vol. 229, pp. 673–681, 2003.

[42] C. Lenglet, J. S. W. Campbell, M. Descoteaux, G. Haro, P. Savadjiev, D. Wassermann, A. Anwander, R. Deriche, G. B. Pike, G. Sapiro, K. Siddiqi, and P. M. Thompson, "Mathematical methods for diffusion MRI processing," *NeuroImage*, vol. 45, pp. S111–S122, 2009.

[43] A. D. Leow, S. Zhu, L. Zhan, K. McMahon, G. I. de Zubicaray, M. Meredith, M. J. Wright, A. W. Toga, and P. M. Thompson, "The tensor distribution function," *Magn. Reson. Med.*, vol. 61, pp. 205–214, 2009.

[44] D. S. Tuch, T. G. Reese, M. R. Wiegell, N. Makris, J. W. Belliveau, and V. J. Wedeen, "High angular resolution diffusion imaging reveals intravoxel white matter fiber heterogeneity," *Magn. Reson. Med.*, vol. 48, pp. 577–582, 2002.

[45] A. Schwartzman, "Random ellipsoids and false discovery rates: Statistics for diffusion tensor imaging data," Ph.D. dissertation, Stanford University, Stanford, CA, 2006.

[46] N. Lepore, C. A. Brun, Y. Chou, M. Chiang, R. A. Dutton, K. M. Hayashi, E. Luders, O. L. Lopez, H. J. Aizenstein, A. W. Toga, J. T. Becker, and P. M. Thompson, "Generalized tensor-based morphometry of HIV/AIDS using multivariate statistics on deformation tensors," *IEEE Trans. Med. Imag.*, vol. 27, no. 1, pp. 129–141, Jan. 2008.

[47] A. Schwartzman, R. F. Dougherty, and J. E. Taylor, "Cross-subject comparison of principal diffusion direction maps," *Magn. Reson. Med.*, vol. 53, pp. 1423–1431, 2005.

[48] H. T. Zhu, Y. S. Cheng, J. G. Ibrahim, Y. M. Li, C. Hall, and W. L. Lin, "Intrinsic regression models for positive definitive matrices with applications in diffusion tensor images," *J. Am. Stat. Assoc.*, vol. 104, pp. 1203–1212, 2009.

[49] B. Whitcher, J. J. Wisco, N. Hadjikhani, and D. S. Tuch, "Statistical group comparison of diffusion tensors via multivariate hypothesis testing," *Magn. Reson. Med.*, vol. 57, pp. 1065–1074, 2007.

[50] Y. Fang and Y. Wang, "Testing for familial aggregation of functional traits," *Stat. Med.*, vol. 28, pp. 3611–3625, 2009.